

Supplementary information

Quantitative 3D Characterization of Elemental Diffusion Dynamics in Individual Ag@Au Nanoparticles with Different Shapes

Alexander Skorikov^{a‡}, Wiebke Albrecht^{a‡}, Eva Bladt^a, Xiaobin Xie^b, Jessi E.S. van der Hoeven^{bc}, Alfons van Blaaderen^b, Sandra Van Aert^a and Sara Bals^{a*}

^aEMAT, University of Antwerp, Groenenborgerlaan 171, 2020 Antwerp, Belgium

^bSoft Condensed Matter, Debye Institute for Nanomaterials Science, Utrecht University, Princetonplein 5, 3584 CC Utrecht, The Netherlands

^cInorganic Chemistry and Catalysis, Debye Institute for Nanomaterials Science, Utrecht University, Universiteitsweg 99, 3584 CG Utrecht, The Netherlands

*To whom all correspondence should be addressed.

E-mail: Sara.Bals@uantwerpen.be

‡These authors contributed equally.

Nanoparticles synthesis

Chemicals

Hydrogen tetrachloroaurate (III) hydrate (HAuCl₄, 99.9%, Sigma), sodium borohydride (NaBH₄, 96%), silver nitrate (AgNO₃, 99.9%), L-ascorbic acid (AA, 99.98%), cetyltrimethylammonium bromide (CTAB, 98%), cetyltrimethylammonium chloride (CTAC, 99%), tetraethyl orthosilicate (TEOS, 98%), hydrochloric acid (HCl, 37 wt % in water) and sodium hydroxide (NaOH, 98%) were purchased from Sigma-Aldrich. Sodium oleate (NaOL, 97.0%) was purchased from TCI America. All chemicals were used as received without further purification. Ultrapure deionized water with a resistivity of 18.2 MΩ·cm at 25 °C was used in all of the experiments.

Synthesis of the mesoporous silica coated Au-core Ag-shell nanorods

The gold nanorods (NRs) synthesis was performed according to the procedure of Ye *et al.*¹ The seed solution consisted of 10 mL 0.10 M CTAB and 51 μL 50 mM HAuCl₄ to which 1.0 mL 0.0060 M NaBH₄ was added while stirring vigorously for 2 min. For the growth solution 7.0 g cetyltrimethylammoniumbromide (CTAB) and 1.24 g sodium oleate were dissolved in 250 mL Milli-Q H₂O. Next, 250 mL 1.0 mM HAuCl₄, 7.2 mL 10 mM AgNO₃, 2.1 mL HCl (37 wt%, 12.1 M), 1.25 mL 0.064 M ascorbic acid and 0.80 mL seed solution were added, while stirring at 350 rpm (revolutions per minute) in a 30 °C water bath. The reaction mixture was left unstirred overnight. Thereafter, the NRs were washed with H₂O *via* centrifugation at 8000 rcf (relative centrifugal force) for 30 min and redispersed in 175 mL 1.5 mM CTAB water solution (LSPR peak position = 853 nm).

The particles were silica coated by following the procedure of Gorelikov *et al.*,² which typically yields a 15-20 nm coating containing 2.5 nm wide mesopores. To the 175 mL 1.5 mM CTAB solution, 1.75 mL 0.1 M NaOH were added while stirring at 300 rpm in a 30 °C water bath. Next, 3 times 525 µL 0.90 M TEOS in ethanol (EtOH) were added with a 45 min time interval. The mesoporous silica coated Au NRs were centrifuged at 8000 rcf for 30 min, washed with water and EtOH and redispersed in 210 mL methanol (MeOH) for subsequent oxidative etching.

The oxidative etching was carried out in MeOH using H₂O₂.³ 100 mL of mesoporous silica coated Au NRs in MeOH (LSPR peak position = 838 nm) were heated in a 60 °C oil bath, while stirring at 400 rpm. 2.0 mL HCl (37 wt%, 12.1 M) and 2.0 mL 50 mM H₂O₂ in MeOH were added. The etching was stopped after 26 minutes (LSPR peak position = 694 nm) by quenching with 100 mL ice cold MeOH. before centrifugation at 10000 rcf for 20 min. The etched rods were washed with and redispersed in 120 mL H₂O.

For the Ag shell growth, we modified the procedure of Deng *et al.*³ To 120 mL aqueous rod dispersion, 1.5 mL 0.10 M HCl, 6.6 mL 5.0 mM AgNO₃ and 6.6 mL 20 mM ascorbic acid in water were added. After 20 minutes, the rods were washed with water and EtOH and stored in EtOH in the dark at 4 °C to prevent oxidation and dissolution of the Ag shell.

Synthesis of the mesoporous silica coated Au-core Ag-shell nanotriangles

The synthesis of Au nanotriangles (NTs) was modified from a previously reported method.⁴ The procedure proceeded in the following steps. (1) 25 µL of 0.05 M HAuCl₄ was mixed with 4.70 mL of 0.10 M CTAC solution in a 20 mL glass vial. Then 0.3 mL of freshly prepared 10 mM NaBH₄ was injected into the mixture described above while stirring. The seeds solution was strongly stirred for 2 min and kept at room temperature for at least 2 hours. (2) 1.60 mL of 0.10 M CTAC, 40 µL of 0.05 M HAuCl₄, and 30 µL of 10 mM KI were added into 8.00 mL of deionized water in a 20 mL glass vial one by one; the resulting solution is named solution A. (3) 30 mL of deionized water was added into a 100 mL flask. 30 mL of 0.1 M CTAC and 0.45 mL of 10 mM KI were injected into the deionized water; the resulting solution is named solution B. (4) 40 µL and 0.6 mL of 0.10 M ascorbic acid solution were injected into solution A and solution B, respectively. As both of solution A and solution B turned colourless, 50 µL of the Au seeds, diluted 10 times in a 0.1 M CTAC solution, was injected into solution A, which was stirred for several minutes after the addition. Subsequently, all of solution A was added into solution B while stirring. The resulting solution were left stirring for at least 2 hours to allow for Au nanocrystals growth. (5) After growing for about 2 hours, 34 mL of B-solution and 4.50 mL of 25 wt% CTAC were mixed in a 50 mL tube, and then keep undisturbed for 12 hours. The excess of CTAC in the form of micelles caused depletion aggregation of the Au NPs. resulting in their sedimentation to the bottom of the tube. The supernatant was removed carefully, while the sediment was suspended in 35 mL of 0.01 M CTAC and served as the NTs stock solution.

In the next step the obtained Au NTs were coated with Ag. 6.30 mL of deionized water and 3.50 mL of Au NTs stock solution were mixed in a 20 mL glass vial, then 0.15 mL of 0.01 M AgNO₃ and 0.1 mL of 0.10 M ascorbic acid were added while stirring the mixture. After reacting at 60 °C for 2 hours, the product was collected by centrifugation at 8000 rpm for 10 min, and then washed by 5 mL of deionized water for one time to remove the of excess CTAC. Lastly, Au NT@Ag particles were collected by centrifugation at 8000 rpm for 10 min, and suspended into 10 mL of deionized water to serve as the Au NT@Ag stock solution.

Finally, the resulting nanoparticles were coated with mesoporous SiO₂. 10 mL of Au NT@Ag stock solution was transferred into a 20 mL glass vial. 100 µL of 0.1 M NaOH was added to the above solution

and 200 μL of 20 v% TEOS in MeOH was injected in one shot under stirring. The resulting solution was kept stirring for 48 hours. After that, the nanoparticles were collected by centrifugation at 8000 rpm for 10 min, washed by 5 mL of deionized water two times and suspended in 0.5 mL of EtOH.

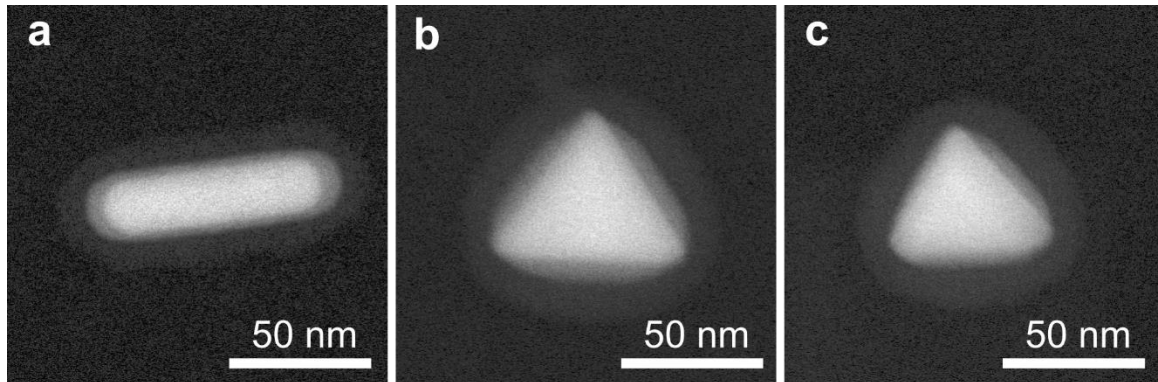


Figure S1. HAADF-STEM images of the studied Au-Ag core-shell particles: (a) nanorod, (b) symmetric and (c) asymmetric nanotriangles.

Derivation of intensity-composition relationship for voxels of 3D HAADF-STEM reconstruction

Since the HAADF-STEM signal is only sensitive to the mass-thickness of the specimen, the intensity of a voxel in the 3D reconstruction of a binary system can be approximated as:⁵

$$I = D_e(N_A\sigma_A + N_B\sigma_B)$$

where D_e is the electron dose received by the voxel, N_i is the number of atoms inside the voxel volume and σ_i is the atomic scattering cross-section for elements A and B. Next, we can use the information about the intensities produced by voxels consisting of pure elements to estimate their atomic scattering cross sections:

$$\sigma_A = \frac{\bar{I}_A}{D_e\bar{N}_A}$$

$$\sigma_B = \frac{\bar{I}_B}{D_e\bar{N}_B}$$

where \bar{I}_A and \bar{I}_B are signals of pure-element voxels, and \bar{N}_i indicates the number of atoms inside a voxel of pure i -th element. Then, we assume that the number of atoms inside the volume of a single voxel does not change during the course of alloying, giving:

$$\bar{N}_A = \bar{N}_B = N_A + N_B = N_{total}$$

This assumption is reasonable if the lattice constant (and thus the total number of atoms per voxel) for the alloy and for the pure elements is the same, such as the case for Au and Ag, used in the present work. Now, we can substitute the atomic scattering cross-sections in the expression of a voxel intensity to obtain:

$$I = D_e \left(\frac{N_A\bar{I}_A}{D_eN_{total}} + \frac{N_B\bar{I}_B}{D_eN_{total}} \right)$$

which simplifies to:

$$I = \frac{N_A \bar{I}_A + N_B \bar{I}_B}{N_{total}}$$

Defining the relative atomic content of an element A as:

$$\omega_A = \frac{N_A}{N_{total}}$$

we can see that the intensity of the voxel can be written as:

$$I = \omega_A(\bar{I}_A - \bar{I}_B) + \bar{I}_B$$

This expression can be used to estimate elemental compositions of arbitrary voxels inside the 3D reconstruction, provided the imaging conditions used to obtain I , \bar{I}_A and \bar{I}_B are kept the same.

Reconstruction of 3D elemental distribution from HAADF-STEM tomography

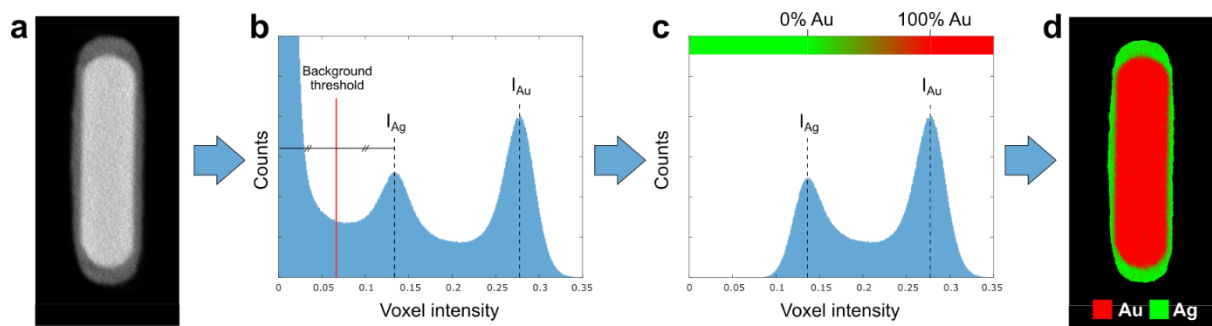


Figure S2. Schematic of elemental distribution calculation method. (a) Slice through a 3D HAADF-STEM reconstruction. (b) Histogram of intensities in the 3D reconstruction. (c) Histogram of intensities after applying vacuum mask. (d) Slice through the calculated 3D elemental distribution.

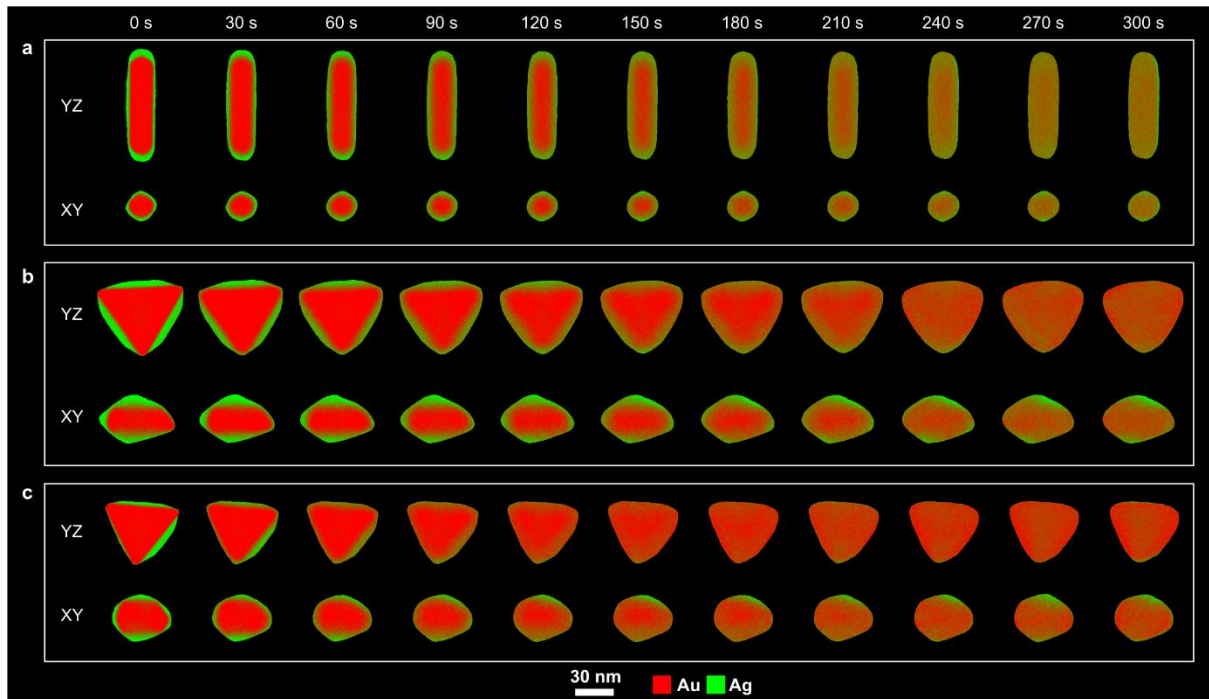


Figure S3. Slices through the calculated 3D elemental distributions in (a) nanorod, (b) symmetric and (c) asymmetric nanotriangles at all alloying times. Slices in two orthogonal planes – YZ and XY – are presented.

3D method for calculating the degree of alloying

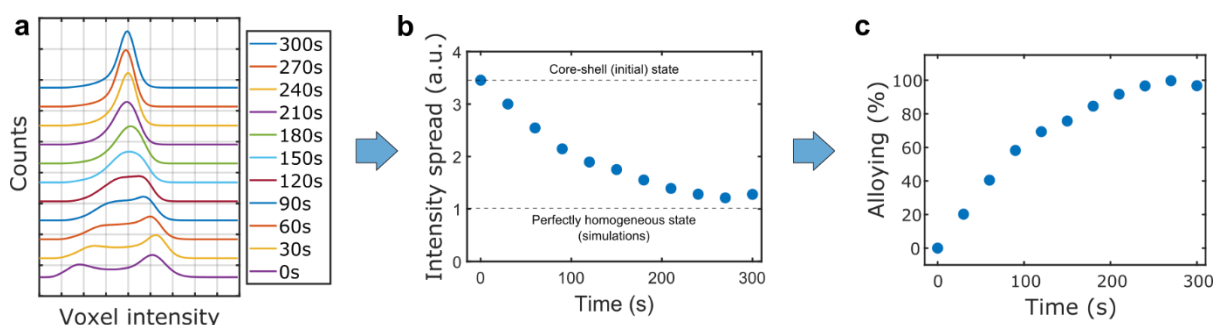


Figure S4. Schematic of the method used to calculate the degrees of alloying. (a) Histograms of voxel intensities in the 3D HAADF-STEM reconstructions for the same particle at different alloying steps. (b) Spreads of the voxel intensity distributions at each step of alloying. Values corresponding to the initial core-shell state and a perfectly homogeneous state simulation are indicated. (c) Alloying curve, obtained by normalizing the values in the time series between the values for the core-shell and the homogeneous states.

Comparison to 2D EDX based method for calculating the degree of alloying

We compared our method to a more conventional approach based on 2D EDX maps.⁶ To obtain quantitative 2D information from EDX, we applied the following steps to the NPs under investigation in this study:

1. Integrated line profiles were obtained from EDX maps for Au and Ag;
2. The profiles were smoothed by applying a moving average filter and the number of counts was normalized between 0 and 1 for each element;
3. Diameter of core and shell were determined by finding the distance between the points corresponding to 0.5 levels for the counts of Au and Ag, respectively;
4. Estimate for the degree of alloying was obtained by scaling the core-to-shell ratios for all time steps between 0% and 100% using the following formulas:

$$R = \frac{d_{core}}{d_{shell}}$$
$$\alpha = 100\% \cdot (R - R_0)$$

where R is the core-to-shell ratio, d_{core} and d_{shell} are diameters of the core and the shell, respectively, α is the degree of alloying, R_0 is the core-to-shell ratio at the initial time step.

Figure S5a illustrates the estimated alloying dynamics for all three particles as obtained by 2D EDX method. It can be seen that the spread in data points is quite large and that no conclusions can be drawn when comparing the three particles. This is especially pronounced for the asymmetrically Ag coated nanotriangle. This is not surprising since 2D projection methods inherently result in less complete information when applied to asymmetric particles. Indeed, the elemental redistribution in some parts may be hidden by using 2D projections only. In addition, the variability of the results obtained from EDX mapping is much higher because of the considerably lower signal-to-noise ratio of the method. This effect is especially important in determining the onset of alloying, which is an important parameter in material science to *e.g.* understand the degradation of materials or changes in optical and magnetic properties.⁷ For the 2D EDX method, alloying does not seem to occur before 100 s, whereas from the 3D data, it is clear that alloying starts right away, in agreement with the 2D slices of the reconstruction (Figure S3).

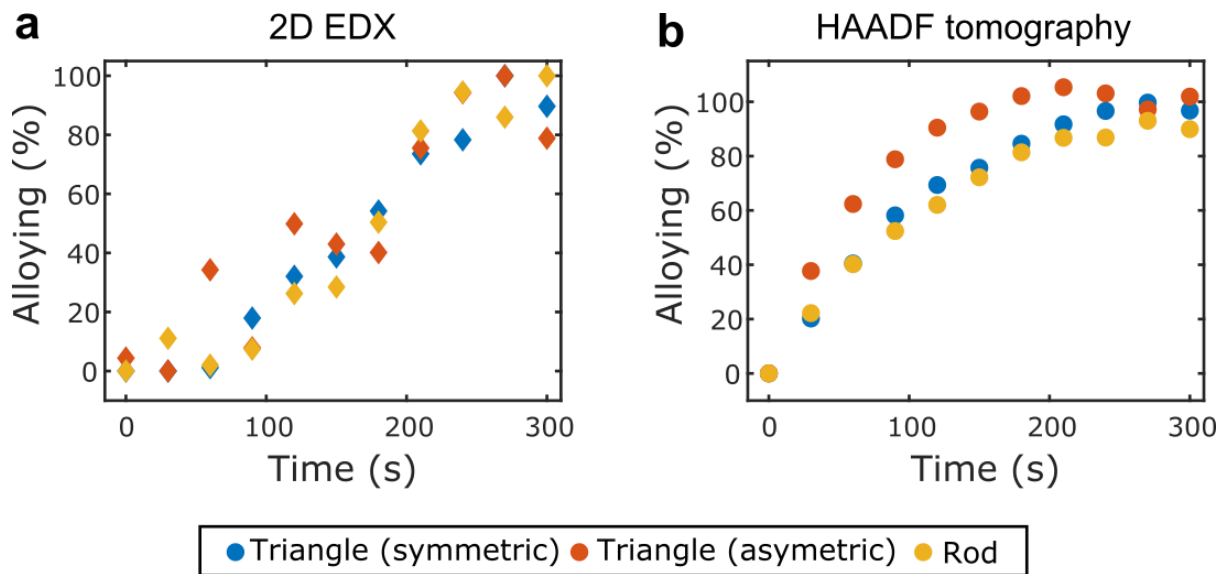


Figure S5. Comparison of the dynamics of alloying for the three particles estimated from (a) 2D EDX elemental mapping and (b) the 3D reconstruction of the compositional distribution.

Diffusion simulations

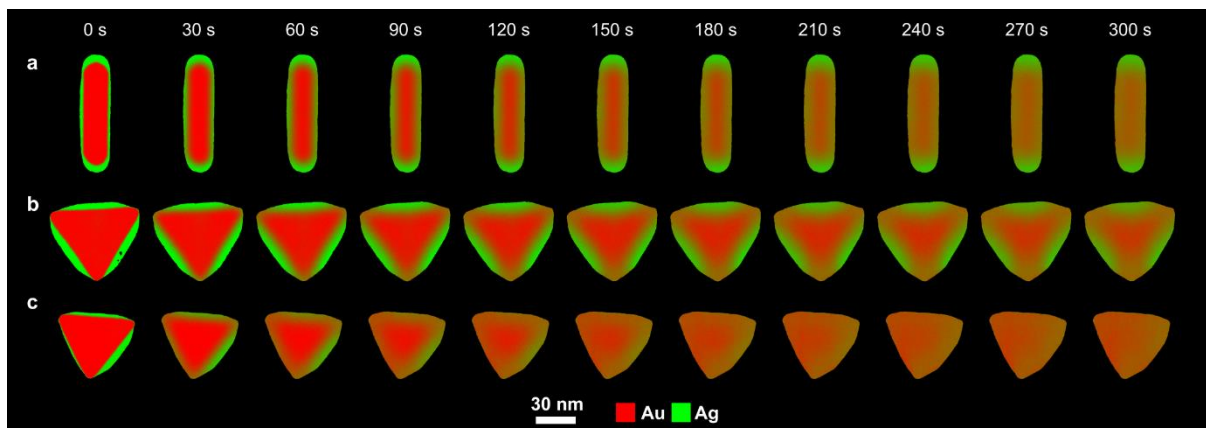


Figure S6. Results of diffusion simulation using the optimal diffusion coefficients. (a) Nanorod, $D = 1 \times 10^{-19} \text{ m}^2/\text{s}$. (b) Symmetric nanotriangle, $D = 1.5 \times 10^{-19} \text{ m}^2/\text{s}$. (c) Asymmetric nanotriangle, $D = 3 \times 10^{-19} \text{ m}^2/\text{s}$.

Reshaping of the studied particles upon heating

Although the studied particles were coated with a thin layer of silica to minimize their deformation during heating, we observed their slight reshaping over the course of alloying. The local volume increase and decrease can be illustrated by superimposing the 3D reconstructions of the particles at the initial and the final stages of alloying (Figure S7). It is visible, that material redistributes from the tips of the particles to the low curvature regions, resulting in a rounder shape at the end of alloying.

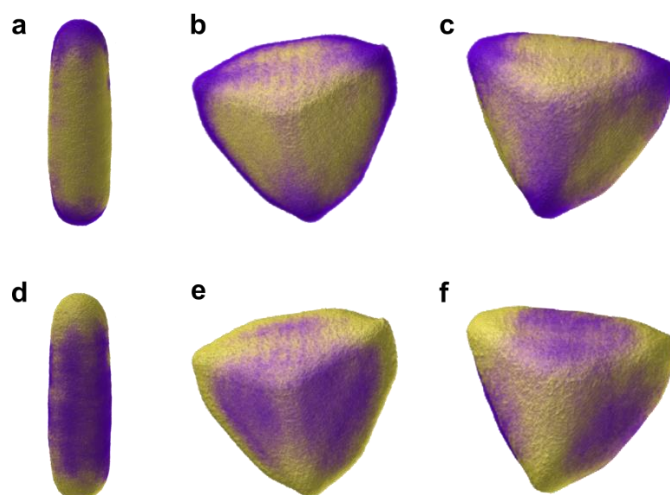


Figure S7. Reshaping of the particles during the heating. Golden colour shows local volume increase (a-c) and decrease (d-f) for the nanorod, symmetric and asymmetric nanotriangles, respectively.

References

- (1) Ye, X.; Zheng, C.; Chen, J.; Gao, Y.; Murray, C. B. Using Binary Surfactant Mixtures to Simultaneously Improve the Dimensional Tunability and Monodispersity in the Seeded Growth of Gold Nanorods. *Nano Lett.* **2013**, *13*, 765–771.
- (2) Gorelikov, I.; Matsuura, N. Single-Step Coating of Mesoporous Silica on Cetyltrimethyl Ammonium Bromide-Capped Nanoparticles. *Nano Lett.* **2008**, *8*, 369–373.
- (3) Deng, T. S.; van der Hoeven, J. E. S.; Yalcin, A. O.; Zandbergen, H. W.; van Huis, M. A.; van Blaaderen, A. Oxidative Etching and Metal Overgrowth of Gold Nanorods within Mesoporous Silica Shells. *Chem. Mater.* **2015**, *27*, 7196–7203.
- (4) Scarabelli, L.; Coronado-Puchau, M.; Giner-Casares, J. J.; Langer, J.; Liz-Marzán, L. M. Monodisperse Gold Nanotriangles: Size Control, Large-Scale Self-Assembly, and Performance in Surface-Enhanced Raman Scattering. *ACS Nano* **2014**, *8*, 5833–5842.
- (5) MacArthur, K. E.; Slater, T. J. A.; Haigh, S. J.; Ozkaya, D.; Nellist, P. D.; Lozano-Perez, S. Quantitative Energy-Dispersive X-Ray Analysis of Catalyst Nanoparticles Using a Partial Cross Section Approach. *Microsc. Microanal.* **2016**, *22*, 71–81.
- (6) van der Hoeven, J. E. S.; Welling, T. A. J.; Silva, T. A. G.; van den Reijen, J. E.; La Fontaine, C.; Carrier, X.; Louis, C.; Blaaderen, A. Van; de Jongh, P. E. *In Situ* Observation of Atomic Redistribution in Alloying Gold–Silver Nanorods. *ACS Nano* **2018**, *12*, 8467–8476.
- (7) Ferrando, R.; Jellinek, J.; Johnston, R. L. Nanoalloys: From Theory to Applications of Alloy Clusters and Nanoparticles. *Chem. Rev.* **2008**, *108*, 845–910.